

Article

Experimental Validation of Seawater Refractive-Index Modeling in the Near-Ultraviolet Band

Siamak Khatibi *  and Fatemeh Tavakoli * 

Blekinge Institute of Technology, 371 79 Karlskrona, Sweden

* Correspondence: siamak.khatibi@bth.se (S.K.); fatemeh.tavakoli@bth.se (F.T.)

Abstract

Accurate knowledge of seawater optical properties is essential for underwater imaging, sensing, and optical communication, particularly in coastal and shallow-water environments where geometric light propagation effects can influence measurement accuracy. While empirical formulations describing the refractive index of seawater are well established and widely used in the visible spectral range, their applicability in the near-ultraviolet region has received limited experimental validation. In this work, the applicability of an established empirical seawater refractive-index formulation in the near-ultraviolet band is investigated through a combined numerical and experimental approach. First, the empirical model is evaluated numerically to examine its spectral behavior across the visible–near-ultraviolet transition. The results indicate smooth and physically consistent refractive-index variation near the ultraviolet boundary. Second, a controlled laboratory experiment is conducted in which near-ultraviolet beam refraction through stratified seawater is measured using a multi-compartment tank designed to emulate discrete ocean depth intervals. Beam displacement measurements at two near-ultraviolet wavelength bands are compared directly with predictions obtained from a multi-layer ray-tracing simulation based on the empirical formulation. The close agreement between simulated and experimentally measured beam displacement across multiple depth configurations provides physical validation of the empirical refractive-index model in the near-ultraviolet region under the investigated conditions. These findings support the use of established refractive-index formulations for near-ultraviolet underwater optical modeling and contribute to a more reliable foundation for near-UV marine optical sensing and measurement applications.

Keywords: seawater optics; refractive index; near-ultraviolet; underwater optical sensing; beam refraction; coastal and shallow waters



Academic Editor: Weicheng Cui

Received: 1 February 2026

Revised: 23 February 2026

Accepted: 25 February 2026

Published: 28 February 2026

Copyright: © 2026 by the authors.

Licensee MDPI, Basel, Switzerland.

This article is an open access article

distributed under the terms and

conditions of the [Creative Commons](https://creativecommons.org/licenses/by/4.0/)

[Attribution \(CC BY\)](https://creativecommons.org/licenses/by/4.0/) license.

1. Introduction

Optical methods play an increasingly important role in the observation, exploration, and monitoring of the marine environment. Applications such as underwater imaging, environmental sensing, bathymetric mapping, and optical communication provide unique advantages over acoustic techniques, including higher spatial resolution and faster data acquisition. These advantages are particularly relevant in coastal and shallow-water regions, where fine-scale spatial information is required for scientific, ecological, and engineering applications [1,2].

As an example of such environments, Sweden's marine waters account for approximately 25–26% of the country's total area, with the Baltic Sea alone representing over 140,000 km² of this extent [3]. The Baltic Sea is a relatively shallow, semi-enclosed basin

with an average depth of about 55 m and extensive coastal and archipelagic zones, where shallow-water light propagation effects are particularly relevant for environmental observation, monitoring, and optical measurement systems [4].

The performance of underwater optical systems is fundamentally governed by the interaction of light with seawater. Absorption and scattering processes have been studied extensively and are known to strongly limit optical range and signal strength [5,6]. In addition to these loss mechanisms, the geometric propagation of light, how optical beams refract, bend, and shift as they traverse water and interfaces, plays a critical role in system calibration, alignment, and quantitative interpretation of measurements. Accurate modeling of light propagation is therefore essential for both the design of underwater optical systems and the interpretation of their data products.

Ultraviolet (UV) and near-ultraviolet wavelengths have attracted renewed attention in marine optics due to their potential advantages in specific applications. Shorter wavelengths can enhance sensitivity to certain biological and chemical constituents, improve spatial resolution in imaging systems, and enable new sensing modalities [6,7]. At the same time, advances in ultraviolet light sources, detectors, and narrowband filtering technologies have made controlled UV and near-UV measurements increasingly feasible in laboratory and field settings. These developments motivate a closer examination of the fundamental optical properties that govern light propagation in seawater at shorter wavelengths.

Among these properties, the refractive index of seawater occupies a central position. The refractive index determines how light rays bend at interfaces, how beam directions evolve within the water column, and how optical paths are mapped between source and detector. In many underwater optical systems, particularly those employing narrow beams, geometric measurement principles, or stratified water columns, small refractive-index variations can lead to measurable beam displacement and systematic effects that must be accounted for to achieve accurate results [1].

Empirical formulations describing the refractive index of seawater as a function of wavelength and environmental parameters have been established and are widely used in ocean-optical modeling. However, these formulations have been developed and validated primarily in the visible spectral range, reflecting the historical focus of optical oceanography and the availability of experimental data. When such models are applied at shorter wavelengths, particularly in the near-ultraviolet region, their validity is often assumed rather than experimentally confirmed.

From a physical standpoint, this assumption warrants careful examination. Optical dispersion increases toward shorter wavelengths, potentially amplifying sensitivity to environmental parameters such as temperature and salinity. As a result, even modest deviations in refractive-index behavior at near-ultraviolet wavelengths could influence beam propagation and measurement accuracy in optical experiments and sensing systems.

The objective of the present work is to address this gap by experimentally examining the applicability of an established empirical seawater refractive-index formulation in the near-ultraviolet spectral region. Rather than introducing a new refractive-index model, this study focuses on physical validation. A controlled laboratory approach is adopted in which near-ultraviolet beam refraction through stratified seawater is measured and compared against predictions derived from the empirical formulation. By linking numerical evaluation with direct beam-displacement measurements, this work provides experimental insight into the consistency of refractive-index modeling at near-ultraviolet wavelengths and contributes to a more reliable foundation for near-UV underwater optical applications.

2. Related Works

The present study lies at the intersection of ocean-optical property modeling, ultraviolet (UV) light interaction with seawater, and underwater optical systems that rely on accurate light propagation physics. While each of these areas has been investigated extensively, their overlap, specifically the experimental validation of seawater refractive-index models in the near-ultraviolet spectral region, has received comparatively limited attention.

2.1. Refractive Index Modeling in Ocean Optics

The refractive index of seawater is a fundamental optical property governing refraction, beam steering, and optical path geometry in marine environments. In ocean optics, refractive index is typically treated as a wavelength-dependent quantity influenced by temperature, salinity, and pressure, and it is routinely incorporated into radiative-transfer models and underwater optical simulations [1].

Empirical refractive-index formulations for seawater have been developed based on laboratory measurements and in situ observations, leading to widely adopted analytical expressions and tabulated datasets. Early work by Austin and Halikas [8] provided foundational refractive-index measurements for seawater, establishing baseline behavior in the visible spectrum [9]. Subsequent studies, notably by Quan and Fry, introduced compact empirical expressions describing refractive index as a function of wavelength, temperature, and salinity, enabling efficient numerical implementation in optical models [10]. Pressure-dependent extensions were later incorporated to support applications at greater ocean depths [11].

These empirical formulations have been validated primarily for visible wavelengths and form the basis of many contemporary underwater optical simulations. However, their applicability outside the original validation range, particularly at shorter wavelengths, is often assumed rather than experimentally verified.

2.2. Ultraviolet and Near-Ultraviolet Light in Seawater

Ultraviolet radiation in the marine environment has been studied extensively, particularly with respect to penetration depth, attenuation, and ecological and biogeochemical impacts. Numerous observational and modeling studies have shown that UV light is strongly attenuated in seawater compared to visible light, with penetration depth depending on water type, dissolved organic matter, and particulate concentration [6,7].

As a result, much of the UV-related ocean-optics literature focuses on absorption and scattering processes, irradiance profiles, and biological exposure rather than refractive behavior. Nevertheless, dispersion effects become more pronounced at shorter wavelengths, implying that refractive-index sensitivity to environmental parameters may increase in the near-ultraviolet region. This provides a physical motivation for reassessing refractive-index modeling at near-UV wavelengths, particularly in experimentally accessible bands close to the visible spectrum.

2.3. Underwater Optical Systems and Propagation Requirements

Accurate modeling of optical propagation in seawater is essential for a wide range of underwater technologies, including imaging systems, laser-based sensing, bathymetric and spectral LiDAR, and underwater wireless optical communication (UWOC). Recent studies have demonstrated the feasibility of high-speed optical communication links underwater using laser sources and advanced modulation schemes, highlighting the importance of precise optical modeling for system design and performance prediction [12,13].

Similarly, underwater LiDAR and optical imaging systems rely on accurate interpretation of beam propagation and interaction with water and interfaces. Investigations

into spectral backscattering, depth-resolved LiDAR returns, and polarimetric underwater imaging illustrate the growing sophistication of marine optical sensing technologies [14,15]. While absorption and scattering dominate signal attenuation in most underwater applications, refractive effects at interfaces and within stratified water columns can influence beam alignment, spot geometry, and calibration accuracy, particularly in narrowband or geometrically sensitive measurement techniques.

2.4. Gap and Motivation for the Present Study

Despite substantial progress in ocean optics and underwater optical systems, direct experimental validation of seawater refractive-index models in the near-ultraviolet spectral region remains scarce. Most established empirical formulations were derived and validated using visible-wavelength datasets, and their extension into the near-UV is commonly performed by extrapolation [10]. Experimental confirmation of such extensions is limited by historical constraints in UV light sources and detectors.

The present work addresses this gap by combining numerical evaluation of an established empirical refractive-index formulation with a controlled laboratory beam-displacement experiment in the near-ultraviolet band. By validating refractive-index behavior at two near-UV wavelength ranges using a stratified, multi-compartment seawater configuration, this study provides physical evidence supporting the applicability of empirical seawater refractive-index modeling beyond the traditional visible spectrum.

3. Refractive Index Modeling and Simulation

3.1. Empirical Seawater Refractive Index Model

The refractive index of seawater is a function of wavelength, temperature, salinity, and pressure (or depth). In this study, the seawater refractive index is evaluated using an established empirical formulation derived from extensive laboratory and field measurements in the visible spectral range. Although this formulation is conventionally applied at wavelengths above approximately 400 nm, its functional dependence on wavelength and thermodynamic parameters provides a physically motivated basis for exploring its behavior in the near-ultraviolet region.

The empirical model is evaluated as a function of wavelength λ , temperature T , salinity S , and depth-dependent pressure. Temperature and salinity values are selected to match the experimental conditions, while pressure is computed from the effective ocean depth represented by each compartment. Particular attention is given to wavelengths between 380 and 425 nm, corresponding to the near-ultraviolet bands investigated experimentally. Following the empirical formulation originally proposed by Quan and Fry [10] and subsequently extended to include pressure dependence by McNeil [11], the refractive index of seawater is expressed as

$$n(\lambda, T, S) = n_0(\lambda) + A(\lambda) T + B(\lambda) S + C(\lambda) T^2, \quad (1)$$

where λ denotes the wavelength in vacuum, T is the seawater temperature, and S is the salinity. The pressure (depth) dependence of the refractive index is incorporated through

$$n(\lambda, T, S, P) = n(\lambda, T, S) + \left(\frac{\partial n}{\partial P} \right) P, \quad (2)$$

where P represents the hydrostatic pressure corresponding to ocean depth. Together, Equations (1) and (2) define the empirical refractive-index model used throughout this study.

3.2. Numerical Assessment of Spectral Continuity

Before applying the empirical refractive-index model to the experimental validation, a numerical assessment was performed to examine its spectral behavior across the visible to near-ultraviolet transition. The refractive index was evaluated over a wavelength range spanning 350 to 450 nm while allowing temperature, salinity, and depth to vary simultaneously within realistic oceanic bounds.

Randomized sampling of the parameter space was employed to capture the combined influence of environmental variability. Specifically, $N = 10,000$ uniform random samples were generated over the ranges $0\text{ }^{\circ}\text{C} < T < 30\text{ }^{\circ}\text{C}$, $33\text{ PSU} < S < 37\text{ PSU}$, $0 < z < 100\text{ m}$, and $200\text{ nm} < \lambda < 400\text{ nm}$. At each wavelength, the resulting refractive-index values were summarized using statistical measures, including median trends and percentile envelopes. This approach enables identification of potential discontinuities or anomalous behavior without assuming validity of the model in the near-ultraviolet region a priori.

The numerical results indicate a smooth and continuous refractive-index variation with wavelength across the visible–near-ultraviolet boundary, supporting the physical plausibility of extending the empirical formulation into the near-ultraviolet band. These results provide the numerical foundation for the subsequent experimental validation.

3.3. Multi-Compartment Ray-Tracing Framework

To establish a direct and physically meaningful link between the refractive-index model and the laboratory measurements, a multi-compartment ray-tracing framework was developed that explicitly replicates the experimental geometry. Rather than approximating the tank as a homogeneous medium with an effective refractive index, the simulation treats the optical path as a sequence of discrete layers corresponding to air, glass walls, and seawater compartments.

The simulated optical path consists of five compartments arranged sequentially along the beam direction, matching the physical tank as illustrated schematically in Figure 1. Each compartment has an internal water-path length of 8 cm, and adjacent compartments are separated by glass walls of thickness 1.5 mm. Glass is modeled using a constant refractive index of 1.50, while air-filled compartments are assigned a refractive index of unity.

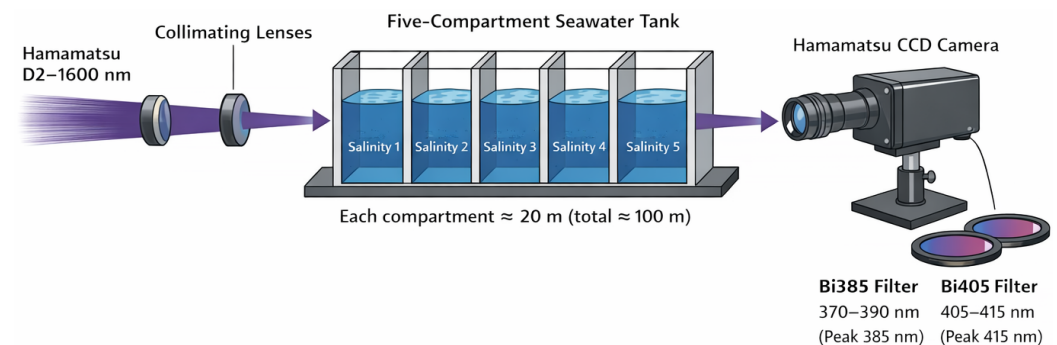


Figure 1. Schematic of the experimental setup used for near-ultraviolet refractive-index validation. A deuterium lamp (200–1600 nm) provides broadband illumination that is collimated and directed into a five-compartment seawater tank arranged sequentially along the beam path. Each compartment provides an 8 cm water path. The compartmental structure enables controlled emulation of layered refractive-index distributions, allowing cumulative multi-interface refraction effects to be investigated under laboratory conditions. The transmitted beam is recorded using a CCD camera (120–1100 nm) with interchangeable interference bandpass filters mounted in front of the camera: Bi385 (370–390 nm, peak 385 nm) and Bi405 (405–415 nm), both from Midwest Optical Systems.

At each interface between adjacent layers, the beam angle is updated according to Snell’s law. The lateral displacement accumulated within each layer is computed from

the local propagation angle and the physical thickness of that layer. The total beam displacement at the exit of the tank is obtained by summing the contributions from all layers traversed by the beam.

3.3.1. Multi-Interface Refraction and Beam Displacement Accumulation

At each interface between adjacent layers, the propagation angle of the beam is updated according to Snell's law,

$$n_i \sin \theta_i = n_{i+1} \sin \theta_{i+1}, \quad (3)$$

where n_i and n_{i+1} denote the refractive indices of the incident and transmitted media, respectively, and θ_i and θ_{i+1} are the corresponding propagation angles measured with respect to the surface normal.

Within each layer k of physical thickness t_k , the lateral beam displacement is computed as

$$\Delta x_k = t_k \tan \theta_k. \quad (4)$$

The total beam displacement at the exit of the multi-compartment tank is obtained by summing the contributions from all traversed layers,

$$X_{\text{total}} = \sum_{k=1}^N \Delta x_k, \quad (5)$$

where N is the total number of air, glass, and seawater layers encountered by the beam along the optical path.

This formulation allows the cumulative refraction induced by sequential seawater compartments and intervening glass walls to be modeled explicitly, rather than approximated using a single effective refractive index.

3.3.2. Model Assumptions and Experimental Correspondence

The ray-tracing model is constructed to replicate the experimental conditions as closely as possible. The number of compartments, their sequential arrangement along the beam path, the internal water-path length of each compartment (8 cm), and the glass wall thickness (1.5 mm per wall) are identical to the physical tank used in the laboratory. Glass walls are modeled using a constant refractive index of 1.50, while air-filled regions are assigned a refractive index of unity.

Each water-filled compartment represents a 20 m ocean-equivalent depth interval, and the seawater refractive index is evaluated at the mid-depth of the corresponding interval using the prescribed salinity and experimental temperature. The incident beam angle is fixed at 0.3° in both simulation and experiment. Under these assumptions, the simulated beam displacement can be directly compared with experimentally measured values without the use of fitting parameters.

3.4. Effective Depth Representation and Salinity Assignment

Specifically, the five compartments represent depth intervals of 0–20, 20–40, 40–60, 60–80, and 80–100 m, with refractive indices evaluated at mid-depths of 10, 30, 50, 70, and 90 m, respectively. Salinity values assigned to each compartment follow the experimental protocol, allowing different stratification scenarios to be reproduced by selectively filling compartments with seawater of prescribed salinity.

This discrete, compartment-based representation enables direct correspondence between simulated and experimental configurations, ensuring that the cumulative refractive effect of layered seawater is modeled consistently in both domains.

3.5. Simulation of Experimental Depth Configurations

The ray-tracing framework is applied to the same four depth configurations investigated experimentally: 60–100 m, 40–100 m, 20–100 m, and 0–100 m. These configurations are implemented by selectively assigning seawater refractive indices to the corresponding compartments while treating the remaining compartments as air-filled regions.

Each seawater-filled compartment represents a 20 m depth interval, and the refractive index is evaluated at the mid-depth of the interval (10, 30, 50, 70, and 90 m). Salinity values assigned to each compartment follow the experimental protocol, allowing the simulation to capture the cumulative refractive effect of stratified seawater layers.

The incident angle of the beam entering the tank is fixed at 0.3° , consistent with the effective experimental geometry. The simulation computes the resulting beam displacement for both near-ultraviolet wavelength bands corresponding to the Bi385 and Bi405 filters.

3.6. Role of Simulation in Experimental Validation

The primary purpose of the simulation framework is to generate quantitative predictions of beam displacement that can be directly compared with experimental measurements. By explicitly modeling the same geometry, materials, wavelength bands, and depth configurations as used in the laboratory, the simulation establishes a one-to-one correspondence between the empirical refractive-index formulation and measurable optical behavior.

Agreement between simulated and experimentally measured beam displacement across multiple depth configurations and wavelengths is interpreted as physical validation of extending the empirical seawater refractive-index model into the near-ultraviolet region. The simulation therefore serves not as an abstract numerical exercise but as an essential component of the experimental validation chain.

4. Experimental Methods

4.1. Experimental Design and Measurement Cases

A series of controlled laboratory experiments was conducted to investigate near-ultraviolet beam refraction in stratified seawater under different effective depth configurations. The experimental design emulates discrete ocean depth intervals using a multi-compartment seawater tank and measures the resulting lateral beam displacement induced by refractive-index variations.

Four experimental configurations were investigated, corresponding to different effective depth ranges: 60–100 m, 40–100 m, 20–100 m, and 0–100 m. Each configuration was realized by filling a selected number of compartments in the tank with seawater of prescribed salinity, while the remaining compartments were left empty (air-filled). In this manner, the experiments represent cumulative refraction through sequential seawater layers of increasing depth.

For each depth configuration, measurements were performed at two near-ultraviolet wavelength bands using narrowband optical filters: a Bi385 interference bandpass filter (370–390 nm, peak transmission near 385 nm) and a Bi405 interference bandpass filter (405–415 nm), both obtained from Midwest Optical Systems, Inc., Palatine, IL, USA. These wavelength bands were selected to probe the near-ultraviolet region where dispersion effects are enhanced and empirical refractive-index formulations are less commonly validated.

Each experimental case was repeated five times under identical optical alignment and exposure conditions to assess measurement repeatability and uncertainty.

4.2. Multi-Compartment Seawater Tank and Optical Configuration

The experimental measurements were performed using a custom-built multi-compartment seawater tank designed to simulate stratified ocean layers. The tank consists of five compartments arranged sequentially along the optical beam path. Each compartment provides an internal water-path length of 8 cm. The compartmental configuration enables controlled variation of refractive index between adjacent layers, thereby producing cumulative multi-interface refraction effects. The laboratory setup does not reproduce physical ocean depth or hydrostatic pressure; rather, it emulates geometric light propagation through stratified refractive-index distributions under controlled conditions. When all five compartments are filled, the total optical path length is 40 cm. Adjacent compartments are separated by glass walls of thickness 1.5 mm. Consequently, as the optical beam propagates through the tank, it undergoes refraction at multiple air–glass, glass–water, and water–glass interfaces. The cumulative beam displacement therefore depends on both the refractive index of seawater within each compartment and the sequence of filled and empty compartments.

Figure 1 illustrates the optical geometry and the sequential multi-compartment tank used to emulate layered seawater conditions, while Figure 2 shows a photograph of the assembled experimental setup.

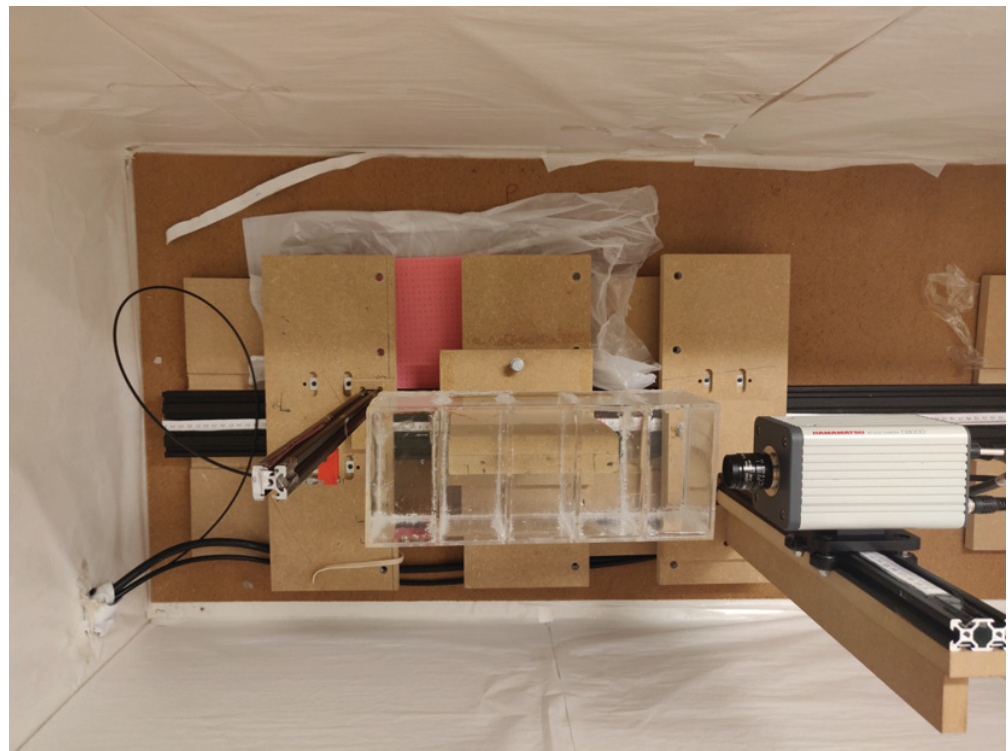


Figure 2. Photograph of the experimental setup used for near-ultraviolet beam-shift measurements. The image shows the broadband light source, collimation optics, sequential five-compartment seawater tank, and the CCD camera positioned downstream of the tank.

A broadband deuterium light source (L10671, Hamamatsu Photonics K.K., Hamamatsu City, Shizuoka, Japan) capable of generating radiation across the ultraviolet and visible spectrum was used as the illumination source. The transmitted beam was detected using a CCD camera (C800-30, Hamamatsu Photonics K.K., Hamamatsu City, Shizuoka, Japan), which provides sensitivity over a wide spectral range including the near-ultraviolet.

The C800-30 camera employs a back-thinned CCD sensor with an effective array of 640×480 pixels and a physical pixel pitch of $14 \mu\text{m} \times 14 \mu\text{m}$. A 25 mm UV-transmitting

fixed focal length lens (C-mount configuration; Edmund Optics, Barrington, NJ, USA) was mounted on the camera. The bandpass filters (Bi385 and Bi405) were positioned in front of the imaging lens to isolate the selected near-UV wavelength band during each measurement. The imaging lens was focused on the exit plane of the final glass interface of the tank. Consequently, the CCD records the lateral displacement of the beam footprint at that plane rather than pure angular deviation at infinity. Although refraction alters the beam angle within the layered medium, the experimentally measured quantity corresponds to spatial displacement at the imaging plane. This ensures consistency between the measured displacement and the ray-tracing predictions.

Narrowband optical filters were mounted in front of the camera to isolate the desired wavelength band during each measurement.

The distance between the tank and both the light source and the camera was kept sufficiently small such that free-space propagation outside the tank could be neglected in the beam-shift analysis. The optical alignment was kept fixed throughout all experiments to ensure that changes in beam position could be attributed solely to refractive effects within the tank. The effective incident angle of the beam at the entrance of the tank was approximately 3° , determined by the fixed alignment of the source, tank, and camera optics, and this angle was maintained consistently across all experimental measurements.

4.3. Image Calibration and Beam-Shift Extraction

Beam displacement was extracted from CCD images using a centroid-based method. To convert pixel displacement into physical units, a geometric calibration procedure was performed.

Calibration images of a checkerboard pattern with known square dimensions of 2×2 cm were acquired using the same camera and optical configuration as in the beam-shift experiments. Intensity profiles across the black and white squares were analyzed to determine the number of pixels corresponding to a known physical distance. For improved accuracy, the calibration procedure was repeated for both horizontal and vertical orientations of the checkerboard.

From the averaged calibration results, a mean value of 136 pixels was found to correspond to a physical distance of 2 cm, yielding a pixel resolution of approximately 0.147 mm per pixel.

It is important to note that this value represents the effective object-plane scaling factor after optical magnification and should not be confused with the intrinsic CCD pixel pitch of 14 μm . The calibrated value of 0.147 mm/pixel therefore corresponds to the spatial resolution in the measurement plane (tank exit plane) rather than the sensor pixel size itself.

Subpixel centroid estimation was employed in determining the beam center, enabling displacement resolution smaller than one pixel and improving measurement precision beyond the nominal object-plane pixel spacing.

This calibrated pixel resolution was subsequently used to convert measured beam centroid shifts into metric units.

Figure 3 summarizes the image acquisition procedure used to isolate the beam displacement caused by the stratified seawater configuration from container-only optical effects. A background image acquired without the tank establishes the reference beam position, an image with the empty tank captures refraction due to the glass walls and geometry, and an image with the tank filled according to a selected depth configuration captures the cumulative refraction induced by the seawater layers. Beam displacement is determined from the centroid shift between the background and filled-tank images under fixed alignment and exposure settings.

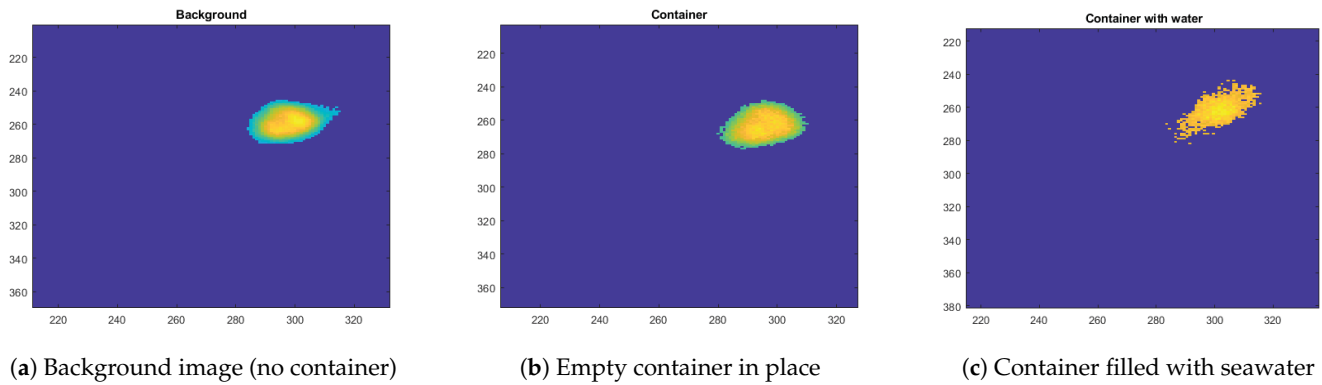


Figure 3. Representative CCD images illustrating the beam-shift measurement procedure. (a) Background image acquired without the physical container, establishing the baseline beam position. (b) Image acquired with the empty five-compartment container in place, accounting for refraction by the container walls. (c) Image acquired with the container filled with seawater, where each compartment contains water of different salinity corresponding to increasing effective depth. Beam displacement is determined from the shift of the beam centroid (or brightest-point location) between the background and filled-tank images under fixed alignment and exposure conditions.

4.4. Measurement Sensitivity to Refractive Index Variations

To assess the sensitivity of the beam-displacement measurement to changes in refractive index, a first-order approximation can be derived from Snell’s law under small-angle conditions.

For an incident angle θ_1 and refractive index n , the refracted angle θ_2 satisfies

$$n \sin \theta_2 = \sin \theta_1. \tag{6}$$

For small angular deviations, $\sin \theta \approx \theta$ (in radians), yielding

$$\theta_2 \approx \frac{\theta_1}{n}. \tag{7}$$

The lateral beam displacement X after propagation through an effective optical path length L is approximately

$$X \approx L \tan \theta_2 \approx L\theta_2. \tag{8}$$

Substituting gives

$$X \approx \frac{L\theta_1}{n}. \tag{9}$$

Differentiating with respect to refractive index yields the first-order sensitivity

$$\frac{dX}{dn} \approx -\frac{L\theta_1}{n^2}. \tag{10}$$

Using the first-order sensitivity relation derived previously in Equation (10), and substituting the experimental geometry ($\theta_1 \approx 3^\circ$, total filled path length $L \approx 0.40$ m, and $n \approx 1.34$), the displacement sensitivity is approximately

$$\left| \frac{dX}{dn} \right| \approx 11.6 \text{ mm per refractive-index unit (RIU)}.$$

This relation provides the theoretical link between measurable beam displacement and refractive-index variations.

4.5. Experimental Displacement Resolution and Minimum Detectable Refractive-Index Change

To quantify the practical displacement resolution of the imaging system, 15 repeated centroid measurements were acquired under identical optical alignment and constant refractive-index conditions. The measured centroid positions (in pixels) were:

305, 305, 304, 306, 305, 305, 305, 305, 305, 305, 306, 305, 305, 305.

The mean centroid position was 305.2 pixels, with a sample standard deviation of

$$\sigma_{px} \approx 0.56 \text{ pixels.}$$

Using the calibrated object-plane scaling factor (0.147 mm per pixel), this corresponds to a physical displacement uncertainty of

$$\sigma_x = 0.56 \times 0.147 \approx 0.082 \text{ mm.}$$

A conservative detection threshold was defined as three times the standard deviation:

$$\delta X_{\min} = 3\sigma_x \approx 0.25 \text{ mm.}$$

Using the displacement sensitivity $|dX/dn| \approx 11.6$ mm per RIU derived in Section 4.4, the corresponding minimum detectable refractive-index change is

$$\Delta n_{\min} \approx \frac{\delta X_{\min}}{|dX/dn|} \approx 0.02.$$

The experimentally determined minimum detectable refractive-index change ($\Delta n_{\min} \approx 0.02$) exceeds the fine-scale refractive-index variations typically associated with realistic salinity and temperature fluctuations at near-ultraviolet wavelengths. Accordingly, the present setup does not resolve small absolute refractive-index differences on the order of 10^{-3} – 10^{-2} . Rather, the experiment validates the cumulative geometric refraction behavior predicted by the empirical model under stratified layered conditions. The agreement between simulation and experiment therefore supports qualitative geometric consistency of the model in the near-ultraviolet region rather than high-precision refractive-index metrology.

5. Results

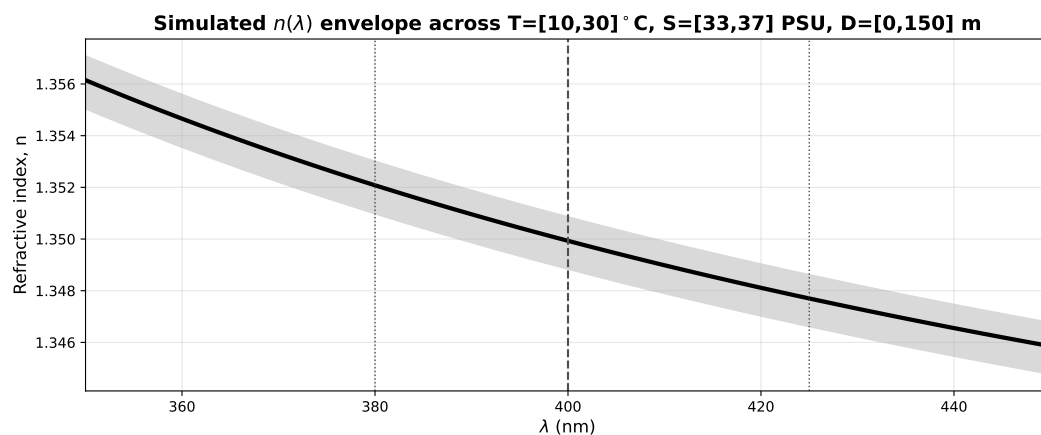
This section presents the results of the numerical–experimental validation performed to assess the applicability of the empirical seawater refractive-index model in the near-ultraviolet spectral region. The results are structured to follow the physical validation chain employed in this study: (i) numerical assessment of refractive-index behavior in the near-ultraviolet, (ii) experimental measurement of beam displacement under stratified seawater conditions, and (iii) quantitative comparison between ray-tracing simulation and experimental observations.

5.1. Numerical Assessment of Spectral Continuity in the Near-Ultraviolet

The empirical seawater refractive-index model was first evaluated numerically to examine its spectral behavior across the visible–near-ultraviolet transition. Figure 4 summarizes the refractive-index variation as a function of wavelength between 350 and 450 nm under simultaneous variability in temperature, salinity, and depth.

The median refractive-index curve exhibits a smooth and continuous variation across the entire investigated wavelength range, including the transition at approximately 400 nm. The bounded percentile envelope indicates that realistic variations in environmental pa-

rameters do not introduce discontinuities or anomalous behavior in the near-ultraviolet region. These results provide numerical support for the physical plausibility of extending the empirical refractive-index formulation into the near-ultraviolet band and motivate subsequent experimental validation.



dispersion behavior across the investigated parameter space.

Figure 4. Simulated absolute refractive index as a function of wavelength across the visible–near-ultraviolet transition (350–450 nm). The solid black line represents the median refractive index computed from 10,000 uniform random seawater conditions with $T \in [10, 30]^{\circ}\text{C}$ and $S \in [33, 37]$ PSU, while the shaded grey region indicates the 5th–95th percentile envelope. The vertical dashed line marks 400 nm, and dotted lines indicate the near-UV band (380–425 nm). The smooth median trend and bounded envelope demonstrate stable and physically consistent dispersion behavior across the investigated parameter space.

5.2. Simulated Reference and Experimental Beam Displacement

Prior to comparison with experimental measurements, the multi-compartment ray-tracing model was used to compute reference beam displacement values as a function of effective depth for the two near-ultraviolet wavelength bands. These simulations were performed using the same compartment geometry, glass wall thickness, and incident angle (0.3°) as in the experiments, but without incorporating experimental measurement uncertainty.

Importantly, these simulated reference values are obtained independently of the experimental measurements and are not fitted to the observed beam displacement. They therefore represent a forward prediction of the expected optical response based solely on the empirical refractive-index model and the known experimental geometry. This predictive role of the simulation is essential for establishing a physically meaningful validation of the refractive-index formulation in the near-ultraviolet region. The simulated reference beam displacement for the Bi385 and Bi405 wavelength bands is shown in Figure 5. The tight vertical axis scaling highlights the small but systematic wavelength dependence, while the weak depth sensitivity reflects the limited variation of refractive index with pressure and salinity over the investigated range.

The simulated reference displacement shown in Figure 5 provides the predictive baseline against which the experimental beam-shift measurements are compared.

For each configuration and wavelength band, five repeated measurements were acquired under fixed optical alignment and exposure conditions. Beam displacement was extracted from the CCD images using the calibrated centroid-based method described in Section 4.3. The mean beam displacement and corresponding standard deviation for each configuration are summarized in Table 1.

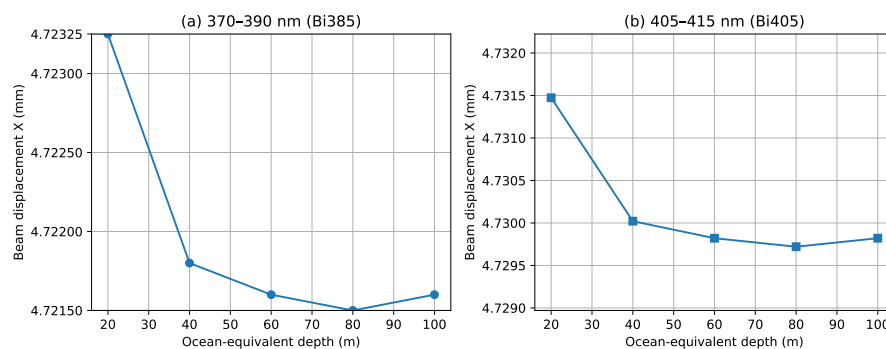


Figure 5. Simulated reference beam displacement as a function of ocean-equivalent depth for near-ultraviolet illumination at $\theta_1 = 3^\circ$ and $T = 24^\circ\text{C}$. (a) Results for the 370–390 nm band (Bi385), using simulated values corresponding to five 20 m depth partitions. (b) Corresponding results for the 405–415 nm band (Bi405), computed using the empirical refractive-index model and Snell’s law. Tight vertical axis ranges are used to highlight the small but systematic variation of the simulated beam displacement with depth and wavelength. Note that θ_1 denotes the effective incidence angle at the first tank interface used in both experiment and simulation.

Table 1. Centroid-based experimental beam displacement measured for different filled-depth configurations of the five-compartment seawater tank. Each compartment represents 20 m of ocean-equivalent depth. Reported values are the mean beam displacement with one standard deviation (SD) obtained from five repeated measurements under fixed optical alignment and exposure conditions.

Filled-Depth Configuration	Bi385 X (mm)	SD (mm)	Bi405 X (mm)	SD (mm)
60–100 m (Compartments 4–5)	1.2273	0.08	1.2836	0.05
40–100 m (Compartments 3–5)	0.2137	0.09	0.3832	0.05
20–100 m (Compartments 2–5)	1.6049	0.06	1.7352	0.07
0–100 m (Compartments 1–5)	3.1458	0.02	3.1867	0.06

The monotonic increase in beam displacement with the number of water-filled compartments reflects the cumulative nature of refraction through sequential seawater layers. Each additional filled compartment introduces an incremental angular deviation at the air–glass and glass–water interfaces, which accumulates along the optical path. This behavior confirms that the measured beam displacement is governed by layered refractive effects rather than by a single effective refractive index, validating the physical relevance of the multi-compartment experimental design.

The experimentally measured beam displacement summarized in Table 1 is interpreted using the simulated reference displacement shown in Figure 2 and forms the basis for the quantitative simulation–experiment comparison presented in Table 2. For all investigated depth configurations, the measured beam displacement at Bi405 is slightly larger than at Bi385, consistent with the expected wavelength-dependent refractive behavior in the near-ultraviolet region.

Table 2. Simulation–experiment comparison of beam displacement for the five-compartment seawater tank at an incident angle of 0.3° . Simulated values are obtained using a multi-interface ray-tracing model that accounts for refraction at each air–glass and glass–(air/water) interface and uses the empirical refractive-index formulation. Absolute error is defined as $|X_{\text{sim}} - X_{\text{exp}}|$.

Filled-Depth	Bi385 (370–390 nm)		Bi405 (405–415 nm)	
	X_{exp} (mm)	X_{sim} (mm)	X_{exp} (mm)	X_{sim} (mm)
60–100 m (Compartments 4–5)	1.2273	1.2723	1.2836	1.2730
40–100 m (Compartments 3–5)	0.2137	0.3000	0.3832	0.3002
20–100 m (Compartments 2–5)	1.6049	1.6911	1.7352	1.6933
0–100 m (Compartments 1–5)	3.1458	3.1651	3.1867	3.1704

5.3. Experimental Beam Displacement Measurements

Prior to comparison, reference beam displacement values were calculated using the multi-compartment ray-tracing model described in Section 3.3. The simulation employed the same optical geometry and incidence angle (0.3°) as in the experiment and was evaluated without incorporating measurement uncertainty.

Importantly, these simulated reference values are obtained independently of the experimental measurements and are not fitted to the observed beam displacement. They therefore represent a forward prediction of the expected optical response based solely on the empirical refractive-index model and the known experimental geometry. This predictive role of the simulation is essential for establishing a physically meaningful validation of the refractive-index formulation in the near-ultraviolet region.

The simulated reference displacement provides a baseline prediction of how beam position is expected to evolve as additional seawater compartments are filled. This reference behavior forms the basis for interpreting the experimental beam displacement measurements summarized in Table 1 and for the subsequent quantitative comparison between simulation and experiment presented in Table 2.

Physically, the simulated reference displacement represents the beam shift that would be observed under ideal measurement conditions if the empirical refractive-index model accurately captures near-ultraviolet refraction in stratified seawater. By computing this displacement prior to comparison with experimental data, the simulation establishes a predictive baseline rather than a fitted response, thereby enabling an objective validation of the refractive-index formulation.

Beam displacement was measured for four filled-depth configurations (60–100 m, 40–100 m, 20–100 m, and 0–100 m) at two near-ultraviolet wavelength bands (Bi385 and Bi405). For each configuration and wavelength band, five repeated measurements were acquired under fixed optical alignment and exposure conditions. Beam displacement was extracted from the CCD images using the calibrated centroid-based method described in Section 4.3. The mean beam displacement and corresponding standard deviation for each configuration are summarized in Table 1. For all configurations, the measured beam displacement at Bi405 is slightly larger than at Bi385, consistent with wavelength-dependent refractive behavior in the near-ultraviolet region.

5.4. Simulation–Experiment Comparison and Validation

To quantitatively validate the empirical refractive-index model, the experimentally measured beam displacements were compared with predictions obtained from the multi-compartment ray-tracing simulation described in Section 3.3. The simulation explicitly accounts for refraction at each air–glass and glass–(air/water) interface and reproduces the exact geometry and depth configurations used in the laboratory. The incident angle was fixed at 0.3° , consistent with the experimental setup.

Table 2 presents a direct comparison between experimentally measured and simulated beam displacement for both near-ultraviolet wavelength bands. For all depth configurations, the simulated beam displacement closely matches the experimental measurements. The absolute deviation between simulation and experiment remains small across all cases, indicating that the cumulative refraction produced by sequential seawater layers is accurately captured by the ray-tracing framework when the empirical refractive-index formulation is applied in the near-ultraviolet region.

The agreement observed across multiple depth configurations and two independent wavelength bands demonstrates that the empirical refractive-index model provides reliable predictions of near-ultraviolet beam refraction under stratified seawater conditions.

5.5. Repeatability and Uncertainty Considerations

The standard deviations reported in Table 1 indicate good repeatability of the experimental measurements. The relatively small measurement variability across repeated trials suggests that the observed differences between simulation and experiment are dominated by systematic factors, such as alignment tolerances, glass wall thickness variations, and centroid extraction uncertainty, rather than by random measurement noise.

Overall, the combined numerical and experimental results provide consistent and physically grounded evidence supporting the extension of the empirical seawater refractive-index model into the near-ultraviolet spectral region.

6. Discussion

The results presented in this study provide experimental insight into the applicability of an established empirical seawater refractive-index formulation in the near-ultraviolet spectral region. By combining numerical evaluation with controlled laboratory beam-displacement measurements, the work addresses a gap between widely used visible-spectrum refractive-index models and their assumed use at shorter wavelengths.

6.1. Consistency of Near-UV Refractive Behavior

A key outcome of this study is the observed consistency between simulated and experimentally measured beam displacement at near-ultraviolet wavelengths. Across all investigated depth configurations, the multi-compartment ray-tracing model produced beam-shift predictions that closely matched the experimentally measured values for both Bi385 and Bi405 wavelength bands. This agreement indicates that the empirical refractive-index formulation exhibits physically consistent behavior when evaluated in the near-ultraviolet region under the investigated conditions.

Importantly, the validation is based on a geometric optical effect, beam refraction and lateral displacement, rather than on indirect fitting or numerical extrapolation alone. The ability of the empirical model to reproduce measured beam shifts through sequential seawater layers provides direct physical evidence supporting its extension beyond the visible spectrum.

6.2. Role of Stratification and Multi-Layer Refraction

The purpose of the stratified multi-compartment configuration is not to increase sensitivity to small refractive-index variations but to reproduce cumulative multi-interface refraction effects consistent with layered shallow-water environments. The layered structure enables direct comparison between experimentally observed beam displacement and ray-tracing predictions derived from the empirical refractive-index model under controlled refractive-index distributions.

The monotonic increase in beam displacement with the number of water-filled compartments reflects the additive nature of refraction across sequential layers. This behavior underscores the importance of accounting for layered refractive effects when interpreting optical measurements in stratified waters. The agreement between simulation and experiment suggests that the empirical refractive-index formulation accurately captures these cumulative effects in the near-ultraviolet regime.

6.3. Wavelength Dependence and Near-UV Sensitivity

A systematic difference between beam displacement measured at the Bi385 and Bi405 wavelength bands was observed, with slightly larger displacement at the longer wavelength. This trend is consistent with wavelength-dependent refractive behavior and supports the physical plausibility of the model in the near-ultraviolet region. Although the wavelength

separation between the two bands is relatively small, the measurable difference highlights the increased dispersion sensitivity at shorter wavelengths.

This sensitivity has practical implications for near-ultraviolet optical systems, where even small refractive-index variations may produce detectable geometric effects. The results suggest that near-UV measurements can serve as a sensitive probe of refractive behavior in seawater, provided that appropriate calibration and modeling are employed.

6.4. Experimental Uncertainty and Model Limitations

While the agreement between simulation and experiment is strong, several sources of uncertainty should be acknowledged. Experimental uncertainties arise from factors such as optical alignment tolerances, glass wall thickness variations, centroid extraction accuracy, and pixel-to-length calibration. These effects contribute to the observed measurement variability and residual differences between simulated and measured beam displacement.

On the modeling side, the empirical refractive-index formulation was evaluated under controlled temperature and salinity conditions representative of the laboratory setup. Natural seawater environments may exhibit additional variability due to spatial gradients, turbulence, and compositional heterogeneity that are not captured in the present experiment. Moreover, the validation is limited to near-ultraviolet wavelengths close to the visible spectrum; extension to shorter ultraviolet wavelengths would require further investigation.

6.5. Implications for Near-UV Underwater Optics

Despite these limitations, the results have meaningful implications for underwater optical research and applications. The demonstrated consistency of empirical refractive-index modeling in the near-ultraviolet region supports its use in optical system design, simulation, and calibration for near-UV underwater sensing. This is particularly relevant for shallow-water and coastal environments, where stratification and interface refraction can influence optical measurements.

By providing experimental validation rather than purely numerical extrapolation, the present work contributes to establishing confidence in near-ultraviolet refractive-index modeling. This foundation is important for future studies that aim to exploit near-UV wavelengths for enhanced sensing sensitivity, fine-scale imaging, or novel marine optical measurement techniques.

6.6. Future Directions

Future work could extend the present approach to a broader range of ultraviolet wavelengths, environmental conditions, and stratification scenarios. Incorporating variable temperature gradients, continuous salinity profiles, and field measurements would further strengthen the applicability of refractive-index modeling in realistic marine environments. Additionally, integrating the validated refractive-index behavior into full radiative-transfer or wave-optics frameworks may provide deeper insight into near-UV underwater optical propagation beyond the geometric regime considered here.

7. Conclusions

This study examined the applicability of an established empirical seawater refractive-index formulation in the near-ultraviolet spectral region through a combined numerical and experimental investigation. By linking refractive-index modeling with direct beam-displacement measurements in a controlled laboratory environment, this work provides physical validation of refractive behavior at near-ultraviolet wavelengths rather than relying solely on numerical extrapolation.

Numerical evaluation of the empirical formulation demonstrated smooth and physically consistent refractive-index behavior across the visible–near-ultraviolet transition.

Building on this result, a multi-compartment laboratory experiment was designed to emulate stratified shallow-water conditions and to measure cumulative beam refraction at two near-ultraviolet wavelength bands. The close agreement observed between simulated beam displacement and experimental measurements across multiple depth configurations provides experimental evidence supporting the geometric consistency of the empirical formulation under the investigated near-ultraviolet conditions.

The results highlight the importance of explicitly accounting for layered refraction in shallow and coastal waters, where cumulative refractive effects can influence optical measurements even when absorption and scattering dominate signal attenuation. The demonstrated consistency between model predictions and experimental observations supports the use of empirical refractive-index formulations for near-ultraviolet underwater optical modeling, system calibration, and interpretation of geometrically sensitive measurements.

While the present validation is limited to near-ultraviolet wavelengths close to the visible spectrum and to controlled laboratory conditions, it establishes a validated foundation for extending refractive-index modeling into this spectral region. Future work may expand this approach to shorter ultraviolet wavelengths, more complex stratification profiles, and field-based measurements, further strengthening the reliability of near-ultraviolet optical techniques in marine environments.

Author Contributions: Conceptualization, S.K.; Methodology, S.K.; Software, S.K. and F.T.; Validation, S.K. and F.T.; Formal analysis, S.K.; Investigation, S.K.; Resources, S.K.; Data curation, S.K. and F.T.; Writing—original draft, S.K.; Writing—review & editing, S.K. and F.T.; Visualization, S.K. and F.T.; Supervision, S.K.; Project administration, S.K. All authors have read and agreed to the published version of the manuscript.

Funding: This research received no external funding.

Data Availability Statement: The original contributions presented in this study are included in the article. Further inquiries can be directed to the corresponding author.

Conflicts of Interest: The authors declare no conflicts of interest.

References

1. Mobley, C.D. *Light and Water: Radiative Transfer in Natural Waters*; Academic Press: Cambridge, MA, USA, 1994.
2. Jaffe, J.S. Underwater optical imaging: The past, the present, and the prospects. *IEEE J. Ocean. Eng.* **2001**, *26*, 683–700. [[CrossRef](#)]
3. Sweden—Marine Waters (Total Area and Breakdown) from Water Information System for Europe. 2024. Available online: <https://water.europa.eu/marine/countries-and-regional-seas/country-profiles/sweden> (accessed on 2 February 2026).
4. Baltic Sea Geography and Characteristics. 2026. Available online: https://en.wikipedia.org/wiki/Baltic_Sea (accessed on 2 February 2026).
5. Jerlov, N.G. *Marine Optics*; Elsevier: Amsterdam, The Netherlands, 1976.
6. Tedetti, M.; Sempéré, R. Penetration of ultraviolet radiation in the marine environment. *Photochem. Photobiol.* **2006**, *82*, 389–397. [[CrossRef](#)] [[PubMed](#)]
7. Huovinen, P.; Ramírez, J.; Gómez, I. Remote sensing of UV radiation in aquatic ecosystems. *PLoS ONE* **2016**, *11*, e0147906.
8. Austin, R.W.; Halikas, G. *The Index of Refraction of Seawater*; Scripps Institution of Oceanography: San Diego, CA, USA, 1976; Ref. 76-1.
9. Li, G.; Wang, Y.; Shi, A.; Liu, Y.; Li, F. Review of Seawater Fiber Optic Salinity Sensors Based on the Refractive Index Detection Principle. *Sensors* **2023**, *23*, 2187. [[CrossRef](#)] [[PubMed](#)]
10. Quan, X.; Fry, E.S. Empirical equation for the index of refraction of seawater. *Appl. Opt.* **1995**, *34*, 3477–3480. [[CrossRef](#)] [[PubMed](#)]
11. McNeil, G.T. Index of refraction of seawater. *Opt. Eng.* **1977**, *16*, 416–420.
12. Xu, J.; Song, Y.; Yu, X.; Lin, A.; Kong, M.; Han, J.; Deng, N. Underwater wireless transmission of high-speed QAM-OFDM signals using a compact red-light laser. *Opt. Express* **2016**, *24*, 8097–8109. [[CrossRef](#)] [[PubMed](#)]
13. Angara, B.R.; Shanmugam, P.; Ramachandran, H. Underwater Wireless Optical Communication System Channel Modelling with Oceanic Bubbles and Water Constituents Under Different Wind Conditions. *IEEE Photonics J.* **2023**, *15*, 7301611. [[CrossRef](#)]

14. Montes, M.A.; Vuorenkoski, A.K.; Metzger, B.; Botson, B. Interpretation of Spectral LiDAR Backscattering off the Florida Coast. *Remote Sens.* **2021**, *13*, 2475. [[CrossRef](#)]
15. Ren, L.; Liang, J.; Qu, E.; Zhang, W.; Du, B.; Ma, F.; Guo, S.; Zhang, J. Polarimetric Optical Imaging: Devices, Technologies and Applications (Invited). *Acta Photonica Sin.* **2022**, *51*, 0851505.

Disclaimer/Publisher's Note: The statements, opinions and data contained in all publications are solely those of the individual author(s) and contributor(s) and not of MDPI and/or the editor(s). MDPI and/or the editor(s) disclaim responsibility for any injury to people or property resulting from any ideas, methods, instructions or products referred to in the content.